Nature Communications

https://doi.org/10.1038/s41467-026-69654-z

Article in Press

Earth system simulations suggest that the Proterozoic ocean was greener but less productive

Received: 15 April 2025

Accepted: 6 February 2026

Cite this article as: Liu, P., Liu, Y., Dong, L. *et al.* Earth system simulations suggest that the Proterozoic ocean was greener but less productive. *Nat Commun* (2026). https://doi.org/10.1038/s41467-026-69654-z

Peng Liu, Yonggang Liu, Lin Dong, Jian Zhang, Sanzhong Li & Yihui Chen

Earth system simulations suggest that the Proterozoic ocean was greener but less productive

Peng Liu[1,2], Yonggang Liu[3*], Lin Dong[4], Jian Zhang[5], Sanzhong Li[1,2], Yihui Chen[3,6]

[1]Frontiers Science Center for Deep Ocean Multispheres and Earth System, Key Lab of Submarine Geosciences and Prospecting Techniques, Ministry of Education and College of Marine Geosciences, Ocean University of China, Qingdao 266100, China.

[2]Laoshan Laboratory, Laboratory for Marine Mineral Resources, Qingdao Marine Science and Technology Center, Qingdao 266237, China.

[3]Laboratory for Climate and Ocean-Atmosphere Studies, Department of Atmospheric and Oceanic Sciences, School of Physics, Peking University, Beijing 100871, China.

[4]Key Laboratory of Orogenic Belts and Crustal Evolution, Ministry of Education and School of Earth and Space Sciences, Peking University, Beijing 100871, China.

[5]State Key Laboratory of Tibetan Plateau Earth System, Environment and Resources (TPESER), Institute of Tibetan Plateau Research, Chinese Academy of Sciences, Beijing 100101, China.

[6]National Satellite Meteorological Center, China Meteorological Administration, Beijing, China

*corresponding author: Yonggang Liu (ygliu@pku.edu.cn)

Abstract

Geological records suggest that marine phytoplankton might have arisen in the Proterozoic while zooplankton remained absent, and marine productivity was not excessively low. However, quantitative estimates of phytoplankton biomass and net primary productivity remain elusive. Here, we use the Community Earth System Model version 1.2.2, modifying biological module and boundary conditions, to simulate marine biogeochemical cycles in the Proterozoic. The simulations demonstrate that, within the expected range of nutrient levels, phytoplankton at sea surface was more than 2 times denser than present, sustaining a greener ocean due to the absence of predators. Heavier surface chlorophyll in the Proterozoic would block sunlight from reaching subsurface layers. This so-called self-shielding effect would decrease subsurface net primary productivity significantly. Simulations show that, through the combined influence of low nitrate level under a low-oxygen environment, the absence of diatoms, and self-shielding, the Proterozoic net primary productivity was only approximately 60% and 30% of the present level in warm (almost ice-free) and cold (sea-ice reaches around 30°N/S) periods, respectively. These findings are subject to uncertainties in model framework and Proterozoic nutrients levels; a slightly less green ocean or more productive ocean was possible if the phosphorus level was much lower or higher than the present level.

MAIN TEXT

Introduction

The Proterozoic Eon covers over 40% of Earth's history from 2500 to 538.8 Ma (million years ago) with its climate being warm in the middle (Boring Billion) but extremely cold near both ends (Snowball Earth events)[1,2]. Based on geochemical and palaeontological records, the primary productivity during the Proterozoic might have been substantial (between ~5% and ~40% of the present-day level)[3,4,5,6]. During the Precambrian, nearly all global productivity was generated by the marine biosphere, while roughly half of productivity came from the land biosphere after the mid-Palaeozoic when vegetation colonized continents[3]. The Proterozoic marine community would primarily be composed of small phytoplankton (e.g., cyanobacteria and green algae), with zooplankton likely absent until the Ediacaran[1,5,7]. The oxygen isotope records indicate that the gross primary productivity during the mid-Proterozoic might have been ~40% of the preindustrial level if the atmospheric oxygen level (pO_2) was 1-10% of the present atmospheric level (PAL)[4], consistent with geochemical simulation results[6]. An active marine biosphere in the Proterozoic could have been important for the evolution of different Earth components. The biological processes may have affected climate by consuming atmospheric CO_2, and (or) injecting organic cloud nuclei into the atmosphere[8,9,10]. The marine photosynthesis is critical for the evolution of the atmospheric as well as marine oxygenation state[11]. The increase in marine productivity and oxygen levels were probably important for the evolution of animals[3]. However, our understanding of the Proterozoic marine biogeochemical cycles is still rudimentary.

The primary productivity in the ocean is largely determined by the variations in temperature, nutrients, and light availability. Other than the large temperature variations, the Proterozoic was also characterized by very different nutrient levels from today due mainly to the low pO_2 at that time. For example, the environment was likely iron rich, supplying abundant iron to the marine ecosystem[12,13]; denitrification would be enhanced in an anoxic ocean[14,15], leading to nitrogen limitation of the primary productivity; the phosphorus (P) level could have also been lower due to limited oxic respiration and (or) removal by minerals[16,17], but some geochemical evidence suggested otherwise[18]. The dimmer Sun during the Proterozoic could have also affected the productivity. Because zooplankton had not appeared during the Proterozoic[1,7], the bloom of surface phytoplankton could have blocked sunlight and suppressed the subsurface primary productivity, just as sometimes observed on the present-day Earth where predators are absent[19,20].

Previous studies involving Proterozoic biogeochemical simulations were based mostly on simplified models such as conceptual models[16,21] and box models[8,22,23]. Recently, an ocean general circulation model has been used to explain the banded iron formations during a Neoproterozoic Snowball Earth event[24]. Although the Proterozoic biogeochemical cycle has been simulated with an atmosphere-ocean general circulation model (AOGCM), that study mainly focused on the role of ocean in modulating the atmospheric CO_2 concentration (pCO_2) and super-greenhouse climate in the aftermath of the Marinoan Snowball Earth event[25]. Therefore, although serving their purposes well, many of the important processes affecting the Proterozoic ecosystem were omitted in the approaches employed by these previous studies. The simplified models could not reveal the spatial structure of the ecosystem while the complex model[25] neglected some of the differences in ecological structure between the Proterozoic and the present, for example, the absence of zooplankton. It is essential to employ an AOGCM that is adapted to the Proterozoic to systematically study its ecosystem.

Here, we use an AOGCM, Community Earth System Model version 1.2.2 (CESM1.2.2), to simulate the marine biogeochemical cycle during both warm (pCO_2=2240 ppmv) and cold (pCO_2=280 ppmv) climate states of the Proterozoic, and compare it to that from a preindustrial (PI) simulation (see Methods). In the cold state, the annual mean sea-ice edges reach ~30° latitude (Fig. 1C), while in the warm state, sea ice is almost absent. Although the continental configuration used here was reconstructed for the late Neoproterozoic (see Methods), the fundamental characteristics of the ecosystem across the entire Proterozoic may have been analogous since the continents remained at relatively low latitudes for the whole eon[26,27]. Moreover, the sensitivity simulations (see Methods) could have covered the uncertainties due to the evolution of continental configuration. Since the diatom and zooplankton were likely absent during the Proterozoic[1,7], we modify the composition of the ecosystem (only consider the small phytoplankton (<20 μm) and diazotroph, following the strategy employed by Gianchandani, et al.[24]; see Methods) and boundary conditions accordingly (see Methods and Supplementary Table 1). Similar simulations were carried out and the climatology analyzed previously by Liu, et al.[28] with the only difference being that the biogeochemical cycle was not turned on. These previous simulations can be compared to the ones performed herein to see the influence of the biogeochemical cycle on the surface albedo. Our model results indicate that, within the expected nutrient regimes, the biomass of phytoplankton in the Proterozoic model setup was higher than that in present-day Earth when predatory zooplankton were absent. Consequently, the denser chlorophyll, causing a greener ocean surface than the present level, would have blocked the subsurface layers from receiving sunlight and reduced the primary productivity there. The total productivity of the Proterozoic ocean simulated by the CESM 1.2.2 was likely lower than that of the present-day ocean.

Results

Greener Proterozoic Ocean. Simulation results show that, without grazing by zooplankton, more phytoplankton would have survived in the upper ocean during the Proterozoic. The global mean chlorophyll averaged within the upper 150 m is 0.10 mg/m^3 in PI (Fig. 1A), similar to the observations[29]. By contrast, the global mean chlorophyll is 0.24 mg/m^3 and 0.15 mg/m^3 during the warm and cold periods of the Proterozoic, respectively (Fig. 1B-C). Moreover, chlorophyll in PI would have varied smoothly over the globe with the majority oceans having values of smaller than 0.15 mg/m^3 (Fig. 1A), while the chlorophyll may have reached >0.3 mg/m^3 over most of the low-latitude oceans in the Proterozoic (Fig. 1B-C). If the permanently ice-covered regions in the cold case are excluded, the mean chlorophyll becomes 0.30 mg/m^3. That is, the simulated concentration of chlorophyll in the upper ocean of the Proterozoic was much higher than that of PI in both the warm or the cold periods. Correspondingly, the plankton carbon within the upper 150 m of ocean was also much higher in the Proterozoic model simulations than in PI (Fig. 1D-F and Supplementary Figure 1).

The model simulations further indicate that the difference in the concentration of chlorophyll within the upper 10 m of ocean between the Proterozoic and PI could have been even more dramatic (Supplementary Figure 2); over regions where primary production is active, the concentration of chlorophyll in the former is generally over 10 times that in the latter (compare Fig. 2A-C and Supplementary Figure 2A-C). During the warm period of the Proterozoic, the primary production may have been active from the equator to approximately 50° latitude (Fig. 2B), covering ~70% of the ocean area; during the cold period, all open ocean (i.e., not covered by sea ice) would have remained production active (Fig. 2C). Therefore, most parts of the simulated Proterozoic ocean would look much greener than the modern ocean (Supplementary Figure 2). The high-latitude oceans of the Proterozoic were barren in life even during the warm period, because the temperature there would still be too low for phytoplankton to flourish while the cold-tolerant diatoms have not evolved yet[30].

The much higher concentration of chlorophyll in the near-surface ocean in the Proterozoic model simulation is primarily due to the absence of zooplankton. In the modern ocean, over 85% of the phytoplanktonic net primary productivity (NPP) is grazed by zooplankton (Supplementary Figure

3A;[31]) and the small phytoplankton contributes only ~50% of the chlorophyll. In contrast, the small phytoplankton contributes ~90% of the chlorophyll in the Proterozoic setup of our model. The rest of the chlorophyll is mainly from diatoms (~45%) and diazotrophs (~10%) in the present-day and Proterozoic, respectively. Due to the absence of grazers, the planktonic carbon can easily reach 3 mmol/m^3 in the upper 50 m and can even be >7 mmol/m^3 (Fig. 1E-F), which is nearly impossible in the modern ocean (Fig. 1D; [32,33]). The small phytoplankton constitutes ~85% of the upper-ocean biomass in the Proterozoic according to the model simulation results while only taking up 40% in the modern. When the zooplankton is added back to the Proterozoic ocean (see Methods for Sensitivity Simulation Group 1 and Supplementary Table 2), surface chlorophyll decreases substantially (Supplementary Figure 4), confirming that the absence of zooplankton was the key trigger of the greener Proterozoic ocean.

Less Productive Proterozoic Ocean. Although the simulated Proterozoic ocean is characterized by more massive phytoplankton, the model results show that its total NPP is less than the PI ocean's. The simulated global total NPP is about 2907 teramoles per year (Tmol/yr) and 1500 Tmol/yr in the warm and cold periods, respectively, ~60% and ~30% of the present level (4754 Tmol/yr) (Fig. 2A-C). The present global mean euphotic depth is about 80 m, defined as the maximum depth at which NPP can occur[34] (Supplementary Figure 5A). But the productive euphotic layer would thin to ~40 m and ~30 m in the warm and cold Proterozic ocean, respectively (Supplementary Figure 5B-C). This smaller total NPP in the simulated Proterozoic is partially due to the absence of diatom because it contributes only 20% of the total NPP in the present ocean; excluding the influence of diatom, the global simulated NPP of the warm and cold Proterozoic ocean is still about 25% and 60% less than that of the present ocean, respectively.

Unlike in the modern ocean where NPP is maintained almost everywhere except the polar oceans (Fig. 2A), NPP is limited to a few zonal stripes in the Proterozoic setup of our model. When the Proterozoic climate is warm, the model results show that NPP concentrates in the equatorial region where upwelling is strong and between roughly 30° and 50° latitudes of both hemispheres where the temperature is still relatively high and vertical mixing is strong[28] with significant iron deposition from dust (Fig. 2B and Supplementary Figure 6A). The NPP in these three latitudinal bands in the upper 20 m of the warm Proterozoic ocean may have been much higher than those in PI (Fig. 2D-E). When the Proterozoic climate is cold, the NPP concentrates in the equatorial region only since the mid-latitude region becomes cold or sea-ice covered (Fig. 2C and 2F), giving a much lower global NPP.

The simulated NPP decreases with depth because of colder and darker ambient conditions, but the rate of decrease could have been much higher in the Proterozoic than in the present ocean (Fig. 2D-F and G-I). For example, the NPP decreases from ~90 to 60 ($\times 10^{-7}$) mmol/m^3/s in the upper 50 m near the equator in the present ocean (Fig. 2D) while it decreases abruptly from ~150 to 10 ($\times 10^{-7}$) mmol/m^3/s in the warm Proterozoic ocean as shown by the simulation results (Fig. 2E). This rapid decrease of NPP with depth should be an important reason why the global total NPP (contributed by small phytoplankton and diazotroph) is lower in the simulated warm Proterozoic than in the present (Supplementary Figure 7), even though the near-surface NPP is much higher (Fig. 2D-F). The massive phytoplankton (chlorophyll, Fig. 1B-C) floating at the surface would have blocked the sunlight from reaching the subsurface and thus decreased the NPP beneath. This phenomenon is termed the self-shielding effect[35,36] as will be discussed in more detail in the next section. However, note that the different nutrient levels between the Proterozoic and PI, especially the marine nitrate (N), are also important for the Proterozoic oceans being less productive than PI oceans (see Discussion).

Self-Shielding Effect. The subsurface ocean of the Proterozoic indeed receives much less sunlight than that of the present simulated by the CESM1.2.2 (Fig. 3A-C and Fig. 4). In the warm Proterozoic scenario, the global mean solar radiation received in the second layer (10 m – 20 m depth) of the ocean is 22.6 W/m^2, about 15 W/m^2 less than the present-day level (Fig. 3A-B). Compared to the warm case, the solar radiation received in the subsurface ocean of the cold case is also low but is relatively high along ~30° latitude and part of the equator. This relatively high value is due to the low NPP and chlorophyll near the sea-ice edges where the temperature is low but the surface radiation is high; the high values along the equator are coincident with the low NPP (Fig. 2C) and chlorophyll (Fig. 1C) there. In fact, the pattern of the subsurface solar radiation in all three cases (Fig. 3A-C) corresponds well with that of the NPP (Fig. 2A-C) and chlorophyll (Fig. 1A-C), indicating that the high surface NPP and chlorophyll are the primary reasons why the Proterozoic subsurface ocean is deprived of sunlight. As described above, the high surface NPP and chlorophyll in the simulated Proterozoic ocean are due to the absence of zooplankton (Supplementary Figure 4).

Whether the self-shielding effect is the reason why the simulated Proterozoic biological productivity is lower than the present can be checked by looking at the major limiting factor of productivity that is output by CESM1.2.2[37]. In the present, N is the most important limiting factor for the growth of small phytoplankton in much of the low to mid-latitudes, except in the South Pacific and Southern Ocean where Fe is the main limiting factor (Fig. 3D), consistent with both observations[38] and other simulation results[29]. During the warm Proterozoic, the simulation results indicate that N is still the dominant limiting factor in the mid-high latitudes due to its much lower deposition rate to the ocean compared to the present (Supplementary Table 1) and the enhanced denitrification effect under the anoxic Proterozoic ocean[14,15] (Supplementary Figure 8). However, in lower latitudes where simulated small phytoplankton flourish (Fig. 1B and 1E) and the surface NPP is high (Fig. 2E), sunlight becomes the most limiting factor (Fig. 3E). For the cold case, the low temperature and sunlight are the most limiting factors in the extratropics and tropics, respectively (Fig. 3F). The fact that sunlight is the most limiting factor for primary productivity in the warm regions of the Proterozoic indicates that self-shielding could have been the major reason for its lower total NPP. The Proterozoic ocean has been thought to be less productive probably due to nutrient shortage (especially N)[16], but here we show that the self-shielding effect, induced by phytoplankton aggregation, could have played an even more important role under the feasible Proterozoic nutrient background (Methods). The simulated greener but less productive Proterozoic ocean compared to the PI regime is summarized in the schematic Fig. 4.

Discussion

Support from modern observations. The simulated greener ocean and related strong self-shielding effect in the Proterozoic are not unimaginable. This phenomenon has also been witnessed in the present eutrophic marginal sea with water bloom and macroalgal abundance[39,40]. In the bloom regions, the surface chlorophyll concentration could increase to ~2-5 mg/m^3 [41,42,43], close to the Proterozoic values simulated by CESM1.2.2 (Supplementary Figure 2B-C). More relevant to the Proterozoic case is the field experiment in the Gulf of Mexico region where the loss of predators (similar to excluding the zooplankton in the Proterozoic simulations) was found to contribute to the overgrowth of phytoplankton and induce self-shielding[44]. The effect of reducing predators on thriving phytoplankton might be more significant than increasing nutrients (e.g., N and P), at least in the northern Gulf district[44]. In the open ocean of North Pacific, the abundance of fish (e.g., salmon and saury) would graze zooplankton and thus enhance the growth of phytoplankton[45,46]. Green of part of Long Lake in Michigan was observed when the largemouth bass was experimentally removed, because it allowed smaller zooplanktivorous fishes to thrive, reducing zooplankton and increasing phytoplankton[20,47]. The shielding effect by surface blooms on the subsurface and benthic primary productivity has also been observed in the modern West Florida shelf and Weeks Bay of Alabama[19,48]. Based on both in-situ and laboratory data, the subsurface NPP in the coastal lagoon near Baltic Sea was believed to be lower due to light limitation caused by a high surface chlorophyll concentration[49]. These observations and fieldwork, although for modern Earth, might provide appropriate bases for our findings herein.

The abundance of small phytoplankton simulated in the Proterozoic would induce a stronger self-shielding effect compared to the modern macroalgal aggregation, because larger phytoplankton has lower light absorption efficiency according to both theoretical[50] and modeling[51] studies. The slower sinking speed of small phytoplankton compared to large algae[52] should also contribute to the greener Proterozoic ocean. Although the rise of algae promoted phagocytosis by eukaryotes during the Neoproterozoic, this process mainly happened in the benthos within the continental shelf[53]. Thus, the phagocytosis may have little grazing effect on the dense phytoplankton in the Proterozoic open surface ocean away from continents as demonstrated in the simulations (Fig. 1B-C).

Other effects of the dense surface phytoplankton (chlorophyll). The simulated dense surface phytoplankton in the Proterozoic ocean has various effects and implications in both biochemistry and climate. 1) The euphotic depth (defined as the maximum depth at which NPP can occur[34]) in the Proterozoic would have been over 50% shallower than the present-day level indicated by the simulation results (Supplementary Figure 5 and Fig. 4); 2) massive surface chlorophyll could have absorbed solar radiation[54] and decreased the regional surface albedo by up to ~2.5% (Supplementary Figure 9A); 3) the stronger absorption of solar radiation at the surface could also have shallowed the mixed-layer depth (Supplementary Figure 9B), reducing ocean-atmosphere exchanges; 4) aerosol emissions by phytoplankton (e.g., dimethyl sulfide and isoprene), which are effective cloud condensation nuclei that modulates cloud properties and climate[55,56], might have been enhanced and played a role in initiating the Neoproterozoic Snowball Earth events[10]. Note that the albedo effect of surface phytoplankton on the global mean surface temperature is very small and the cloud effect of biogenic aerosols is not simulated in this study. Thus, further studies are warranted to investigate the interaction between clouds, climate, and marine biogeochemistry in the Proterozoic.

Uncertainties in the simulated surface greening and NPP. It should be noted that the model framework employed in this study is subject to uncertainties. Whether these uncertainties affect the main conclusions herein are discussed in what follows. Firstly, we show that the dimmer Sun during the Proterozoic is not the reason for the limited subsurface light availability; increasing the solar luminosity to the present strength (see Methods for Sensitivity Simulation Group 2) has little influence on the surface greenness and NPP of the ocean (Supplementary Figure 10).

Secondly, the uncertainty in the vertical diffusivity, which affects nutrient availability, does not affect the main conclusions. Increasing (decreasing) vertical diffusivity parameters by ~53% (24%) in warm Proterozoic simulation (see Methods for Sensitivity Simulation Group 3) would increase (decrease) the NPP by ~22% (17%) (Supplementary Figure 11A-B) compared to the default simulation (Fig. 2E). Stronger vertical mixing would alleviate nutrient limitation and increase NPP (still lower than the present-day value; Supplementary Figure 11C-D) but the reconstructions of both day length[57] and orbital cycles[58] suggest that the tidal dissipation during the Proterozoic was likely much weaker than during the Phanerozoic. In the meantime, the simulated greener Proterozoic surface ocean and related self-shielding effect are unaffected (Supplementary Figure 11E-F).

Thirdly, the uncertainty in nutrients levels, specifically, the levels of N, P, and iron (Fe), do affect the surface greenness and NPP of the Proterozoic but the main conclusions should stay intact for the expected range of nutrients levels. For N, although the initial marine nitrate concentration is set to the present level, it achieves a new equilibrium level quickly with the specified boundary conditions. The boundary condition that affects N the most is pO_2 because denitrification using nitrate will be triggered once the O_2 concentration in the ocean is lower than some threshold (0.1 μmol/L in CESM1.2.2). For pO_2=1% PAL, used in all simulations presented above (Supplementary Table 1), the oceanic and sedimentary denitrification is indeed much stronger than in PI (Supplementary Figure 8D-F and Supplementary Figure 12) and the final nitrate reservoirs are suppressed by over three orders of magnitude through enhanced denitrification (Supplementary Figure 8A-C). Such phenomenon has also been demonstrated by previous field observations and simulations[14,15]. Thus, N is expected to be an important limiting factor for the Proterozoic ecosystem (Fig. 3E-F). If pO_2 is increased to 10% PAL (see Methods for Sensitivity Simulation Group 4), the simulation results show that the denitrification effect is reduced substantially, NPP increases but by only ~7% compared to pO_2=1% PAL scenario (Supplementary Figure 13). When pO_2 is reduced to 0.1% PAL, the surface greening and self-shielding effect are still strong (Supplementary Table 3). Thus, the uncertainty in N does not affect the main findings here.

For P, it turns out its initial reservoir is too large to be affected by the specified Proterozoic boundary conditions (Supplementary Table 1) during the simulations (Supplementary Figure 14), thus additional sensitivity simulations with different initial P concentration have to be carried out (see Methods for Sensitivity Simulation Group 5). Geochemical records indicate that the Proterozoic P could have been 500% to 2.5% of the present oceanic level (POL)[17,18,59]. Simulation results show that a much greener Proterozoic ocean would have been obtained if P is increased to 200% and 500% POL (Supplementary Figure 15A-B) with even stronger self-shielding effect and shallower productive layer (Supplementary Figure 15G-H). The simulated global total NPP at P=200% POL is still lower than that in PI; only when P is increased to 500% POL, the simulated total NPP is larger than PI (Supplementary Figure 15G and Supplementary Table 3). On the other hand, even though NPP is reduced to one sixth of the PI value when P is reduced to 25% POL, the simulation results show that the mid- to low-latitude ocean surface remains slightly greener than the PI ocean surface (Supplementary Figure 15D and Supplementary Table 3). Thus, the Proterozoic ocean would have been greener but less productive unless P was more than twice or less than one fourth of the PI level (i.e., 1 POL).

For Fe, sensitivity simulations (see Methods for Sensitivity Simulation Group 6) show that even when atmospheric and riverine dust inputs are completely removed, and the Fe from ocean bottom is reduced to 10% of the present strength, a much greener ocean can still be maintained (Supplementary Figure 16E). This means that the uncertainty in Fe has almost no influence on our main findings. Therefore, these sensitivity tests indicate that the Proterozoic ocean would have been greener but less productive for the expected nutrient ranges (25% POL < P < 200% POL, and loose ranges for N and Fe) of nutrients levels.

Deficiency in the oxygen cycle. The oxygen cycle in CESM1.2.2 suffers from a few problems which prevent us from letting pO_2 evolve freely and has to be prescribed. If we let pO_2 evolve freely, the large simulated oxygen outgassing flux from the ocean would double it in a few thousand years if the initial pO_2 is 1% PAL. This timescale will lengthen to ~17000 years when pO_2 is increased to 10% PAL (see Methods for Sensitivity Simulation Group 4; Supplementary Table 3). This excessive O_2 from the model is due to deficiency in both the source and sinks. For the source, the oxygen production rate by photosynthesis may have been overestimated for the Proterozoic by the model because several enzymes for catalyzing oxygen production have not evolved[60,61]. For sinks, both the influence of marine (e.g., SO_2 and H_2S) and terrestrial (e.g., FeS) reducers are absent. The remineralization in the seawater is parameterized with the present marine oxygenation and decoupled with the calculated O_2 concentration, so the oxygen sink in the anoxic Proterozoic ocean may have been largely overestimated[62]. Moreover, the refractory dissolved organic carbon (DOC), which may increase oxygen outgassing, is omitted in the model we use[63]. Fortunately, such deficiency in the modeling of oxygen cycle should not interfere with the primary productivity of the near-surface ocean (Supplementary Table 3).

In summary, our model results suggest a greener Proterozoic ocean due to the absence of predators and in the meantime a less productive ocean due to absence of diatoms, the low N nutrient level under low pO_2, and strong self-shielding effect (Fig. 4). It is noted that a less green or more productive Proterozoic ocean might be plausible when the phosphorus level was less than one fourth or more than twice of the PI level, respectively. Whether cold or warm, the surface concentration of chlorophyll of the Proterozoic ocean in ice-free regions was about 2.4 and 3.0 times that of the present-day counterpart under the Proterozoic model setup (Supplementary Table 1). The simulated thriving marine phytoplankton might be a reasonable explanation for the observed fossil records and putatively substantial primary production[3,4,5,6]. Even when the sea ice has developed to near the tropical regions, the regional chlorophyll in the open ocean could still reach 0.5 mg/m^3, which is similar to what is observed in the modern bloom areas. The heavily concentrated surface phytoplankton would have absorbed and blocked radiation from reaching the ocean layer beneath, inducing the so-called self-shielding effect. This effect makes sunlight the most limiting factor for phytoplankton growth. The simulated greener Proterozoic ocean surface lowers the sea surface albedo and increases surface ocean stratification; it could also have effects on climate by releasing more cloud condensation nuclei to the atmosphere. These may be important for understanding the geological records and coevolution of climate and marine biogeochemistry in the deep-time Earth.

Methods

Model Description. To simulate the marine biogeochemical cycle during the Proterozoic, the Community Earth System Model version 1.2.2 (CESM 1.2.2) has been employed in this work which has been broadly used in the deep time simulations[64,65]. CESM1.2.2 includes six components, namely atmosphere, ocean, land, sea ice, land ice, and rivers, which interact with each other through a coupler[66]. The land ice component is not activated in this study. The atmosphere and land components are both operated on the T31 grid with a horizontal resolution of 3.75º×3.75º. The ocean component (Parallel Ocean Program version 2, POP2)[67] and sea ice component are operated on the g37 grid with a uniform 3.6º spacing in the zonal direction and variable spacing (0.6º-3.4º) in the meridional direction. The atmosphere and ocean have 26 and 60 layers in the vertical direction, respectively.

For the horizontal diffusion, the anisotropic mixing of momentum[68] and Gent and Mcwilliams[69] parameterization, which drives the mixing of tracers along isopycnal surfaces with activated submesoscale mixing, has been employed in the model. In the 720 Ma continental configuration used here, the vast ocean without continents in the mid-high latitudes of the Northern Hemisphere would give rise to excessively strong westerly ocean currents (~70 cm/s with ~20° meridional width), warranting higher tracer diffusivities than the default[70]. Thus, we have increased the horizontal diffusivity (variable ah in the model) by a factor of 5 (from 800 m^2/s to 4000 m^2/s), as employed in previous work using the same continental configuration and resolution[28,70]. For vertical mixing, the K-profile parameterization (KPP) has been used in POP2, in which the interior mixing coefficients are computed at every grid point according to relevant physical processes[71]. These physical processes include surface wave breaking, shear instability, convection, background internal wave breaking, and tidal dissipation. For the present-day, the background internal wave breaking is prescribed to a universal constant (also represented by vdc1 with a value of 0.16 cm^2/s), and the tidal dissipation is horizontally variable and decreases exponentially from the bottom to the top. In the deep-time simulations, because the tidal dissipation is unknown, the background and tidal dissipation together (κ) are represented by a function that depends on depth (z) only,

$$\kappa = \text{vdc1} + \text{vdc2} * \tan^{-1}[(z\text{-}1000\text{ m}) * 4.5\times10^{-3}\text{ m}^{-1}] \quad (1)$$

where vdc1 = 0.524 cm^2/s and vdc2 = 0.313 cm^2/s as recommended by NCAR-suggested deep-time standards and previous work[28,72].

For the purpose of this study, the biogeochemical elemental cycling (BEC) model embedded in POP2 has been activated which consists of the upper ocean (0-150 m) ecological and full-depth biogeochemical dynamics[37,73]. The internal sources and sinks of carbon (C), oxygen (O_2), phosphorus (P), nitrogen (N), silicate (Si), and iron (Fe) in BEC, are driven by three functional groups of phytoplankton and one zooplankton. Higher-trophic-level predators and heterotrophic bacteria have been implicitly resolved by the parameterized loss terms associated with zooplankton and scavenging of organic matter, respectively[37,73]. The trophic complexity (phytoplankton–zooplankton–detritus) of type-based BEC is relatively competitive among marine biogeochemical models employed in Phase 5 and 6 of the Coupled Model Intercomparison Project (CMIP5 and CMIP6)[74]. The phytoplankton groups, grazed by the zooplankton, include (pico/nano calcareous) small phytoplankton (<20 μm), N-fixing diazotroph, and diatom. Here, only the former two phytoplankton groups have been involved in the simulations, because the diatom and zooplankton are not believed to have evolved until the end of the Permian[30] and Ediacaran[7], respectively. Moreover, the biomass of large phytoplankton (e.g., dinophyta) is less than that of small phytoplankton and contributes limited NPP in the modern Earth, thus typical marine biogeochemical models always omit various types of large phytoplankton[29,74]. Although the primary marine phytoplankton community might be cyanobacteria during the Proterozoic, the metabolite and biomass (e.g., $H:C_{organic}$ and $O:C_{organic}$ ratios) contents are similar to those of modern phytoplankton[75,76,77]. Thus, the model strategy of ecosystem simplification based on the modern Earth has been widely employed in the simulations of Neoproterozoic[24] and Permian[78] biogeochemistry.

The organic carbon in the ocean, mainly in the form of dissolved organic carbon (DOC) and particulate organic carbon (POC), is consumed by a few remineralization processes in the model and the rest is permanently buried into the seafloor. These remineralization processes include the direct oxidation by oxygen in the seawater, the denitrification in both seawater and the sediments[79,80], and the remineralization by ferric iron, manganese oxides, and sulphate. The anoxic remineralization utilizing these latter three oxidants is lumped into one process in CESM1.2.2, and its flux is formulated to be equal to the organic carbon flux at the seafloor minus the POC settled into sediments and organic carbon consumed by denitrification[80]. The settling fluxes of particles are parameterized based on the marine production, particle aggregation, and physical processes of seawater (e.g., advection)[37,73]. A maximum burial efficiency of 80%[81] is imposed to this POC flux at the seafloor, and the buried organic matter is lost instantaneously from the ocean domain. To avoid drift of the ocean nutrient inventories, an additional input of nutrients is needed to balance the loss of nutrients by this POC burial[73,82]. That is, the nutrients lost due to the permanent burial of these POC are put back to the ocean also instantaneously. The BEC model has been shown to perform well based on a wide range of metrics for the studies of the present[83,84] and paleo Earth[78].

The silicate weathering model, employed for the boundary condition settings in BEC, is essentially the same as that in Park, et al.[85] but with improvement to reduce the bias in global total weathering flux[65,86]. This model considers the processes of regolith generation and physical erosion in the vertical depth and is thus capable of reflecting the influence of supply-limit and kinetically limited conditions simultaneously[87]. The silicate weathering rate depends on the surface temperature, runoff, surface slope, and lithology, with the former two simulated in CESM1.2.2, while the latter two have been set as described in the next section.

Boundary Conditions for the standard simulations. The continental configuration employed here is appropriate for 720 Ma in the Proterozoic[27] with slight modification to increase model stability[28,70]. Due to the lack of surface topography reconstruction and the understanding that the surface of deep-time Earth was generally smooth[88], the surface is assumed to be basically flat. The land surface is set to desert since plants had not colonized the continents during the Precambrian[89]. The solar constant is set to 1285 W/m^2, 6% weaker than the present value[90]. Atmospheric oxygen concentration (pO_2) is prescribed at 1% PAL (PAL: present atmospheric level) with globally uniform distribution and then BEC calculates the dissolved oxygen in the ocean based on Henry's law and relevant piston velocity for the marine biogeochemical simulations[11]. The climate effects of atmospheric aerosols might be significant[13,91] but beyond the scope of the current study, and thus are omitted in the atmosphere model. The orbital parameters are assumed to be those of the year 1990; the concentrations of CH_4 and N_2O are prescribed to be 805.6 and 276.7 ppbv, respectively, as those in the preindustrial. All the settings above are similar to those in previous modeling studies of the Snowball Earth events[28,70]. To be consistent with Liu, et al.[28] so that many of the BEC-induced changes (e.g. mixed-layer depth) can be calculated, atmospheric dust in the atmosphere model is assumed to be zero. To simulate the marine biogeochemical cycle during the Proterozoic in both warm and cold periods, two experiments are carried out in which pCO_2 is set to 2240 and 280 ppmv, respectively.

The boundary conditions of BEC include the nutrients deposited from the atmosphere and injected by runoff into the ocean. Because dust is an important source of Fe for marine life[92], the spatial distribution of dust deposition from a previous simulation is prescribed. Specifically, we use the results of Liu, et al.[91] from the experiment in which pCO_2=280 ppmv and surface erodibility=0.01875 (Supplementary Figure 6A). In this simulation, the amount of dust deposition over the ocean was about 6 times the present level. The Fe is assumed to be 3.5% of the dust mass, 0.8% of which is bioavailable based on models and observations[93,94]. The nitrogen deposition input in BEC contains NO_y (e.g., NO, NO_2, and HNO_3) and NH_x (e.g., NH_3 and NH_2). During the Precambrian, the natural NO_y came from the volcanoes and photochemical reactions under a low oxygen level[95,96]. Here we borrow the NO_y deposition rate (3.52×10^8 kg/yr) from the photochemical simulations in which the N_2O outgassing rate is set to 1 PAL while pO_2=1% PAL[97]. The pO_2 has varied from about 0.001% to 10% PAL during the Proterozoic[11], but the 1% PAL pO_2

state may cover most Meso-Neo Proterozoic[11] and thus has been selected here. Meanwhile, the primary source of NH_y should be NH_3 from volcanos and NH_2 generated by the subsequent photochemistry, both of which are highly soluble. The present NH_3 volcanic outgassing rate (3.72×10^7 kg/yr) is used as the deposition rate of NH_y for the Proterozoic following the strategy in Kasting and Walker[95]. Both NO_y and NH_x deposition rates are about one order of magnitude lower than the present level due to the lack of biota sources (e.g., agriculture and biomass burning) with globally uniform distribution in the Precambrian[98].

The riverine inputs of nutrients to the ocean include dissolved inorganic carbon (DIC), dissolved organic carbon (DOC), dissolved inorganic phosphorus (DIP), dissolved organic phosphorus (DOP), dissolved inorganic nitrogen (DIN), dissolved organic nitrogen (DON), dissolved silicate (DSi), dissolved iron (DFe), and alkalinity (ALK), which should all be specified according to Proterozoic conditions. Due to the barren continents during the Proterozoic, the organic components (i.e. DOC, DOP, and DON) in runoff are neglected herein. Similarly, the majority of DIN in modern runoff originates from nitrogen fixation by terrestrial life[99] as there is little nitrogen in basic rocks[100], and thus DIN can also be omitted here. The DSi is set to zero because diatoms have not yet emerged. The DFe in runoff is fixed to 1.5 Tmol/yr based on the biogeochemical model for the low pO_2 Precambrian[101]. The weathering rates (WR) are calculated by the weathering model described above, assuming a uniform felsic (acid volcanic rock) lithology and using the climate fields from the simulation (with pCO_2=2240 and 280 ppmv) of a previous study[28]. The global total DIC and ALK are calculated to be equal to twice the calculated weathering rate[85]. DIP is assumed to be 0.0382% of the weathering flux based on fieldwork for the acidic volcanic rocks[102]. The spatial distribution of DIC, DIP, DFe, and ALK fluxes are scaled by the pattern of simulated runoff flowing into the ocean in CESM1.2.2 (Supplementary Figure 6B-C)[28]. All the boundary conditions are summarized in Supplementary Table 1. Due to the lack of globally gridded reconstructions for biogeochemical variables during the Proterozoic, their initial values are set to the present level, and will evolve to new equilibrium state under the boundary conditions above. All simulations were continued for 3,500 years so that both the climate and the biogeochemical cycle (e.g., the total NPP, DIC, and DOC) reach an equilibrium state, and the final 100 years are averaged for analyses.

Sensitivity Simulation Groups. Six groups of sensitivity simulations have been carried out to estimate the influence of uncertainties in boundary conditions or model components to the main conclusions drawn from the standard simulations described above. (1) Inclusion of zooplankton in the Proterozoic. The zooplankton has been involved in the ocean simulation with the other boundary conditions the same as those in the pCO_2=280 ppmv simulation. (2) Increase of Proterozoic solar constant. Based on the warm Proterozoic simulation, the solar constant is set to the present level with 280 ppmv pCO_2 so that the climate state is similar to that of the warm standard simulation, while all other boundary conditions (e.g., nutrients) are identical to those in the warm simulation. (3) Variation in the vertical diffusivity. The vertical diffusivity (variable vdc1 in the model) has been increased to 0.8 and decreased to 0.4 cm^2/s for the high and low vertical mixing scenarios[103], respectively, based on the pCO_2=2240 ppmv simulation. (4) Different atmospheric oxygen levels (pO_2). The pO_2 is set to 0.1% and 10% of the present level in the pCO_2=2240 ppmv simulation. (5) Varying the phosphate reservoir. The marine phosphate level has been set to 500%, 200%, 50%, 25%, 10%, and 2.5% of the present oceanic level, with other conditions identical to those in the original pCO_2=2240 ppmv simulation. (6) Lower iron input. This group includes five simulations. In the first one, the sources from the atmospheric dust deposition and riverine input are removed, so that only Fe input through the ocean bottom is considered. In the other four simulations, the Fe from ocean bottom is further reduced to 50%, 25%, 10%, and 0% of the present level. The above boundary conditions for the sensitivity tests are summarized in Supplementary Table 2.

Data Availability

The simulation results used for the present study are archived on Zenodo with the identifier https://doi.org/10.5281/zenodo.18489467. Source data are provided as a Source data file.

Code Availability

The source code of CESM1.2.2 can be accessed at https://github.com/ESCOMP/CESM. The NCAR Command Language (NCL) version 6.2.2 (https://doi.org/10.5065/D6WD3XH5) is used for graphing.

References

1. Hoffman, P. F. et al. Snowball Earth climate dynamics and Cryogenian geology-geobiology. *Sci. Adv.* **3**, e1600983 (2017).
2. Kasting, J. F. Methane and climate during the Precambrian era. *Precambrian Res.* **137**, 119-129 (2005).
3. Butterfield, N. J. Proterozoic photosynthesis–a critical review. *Palaeontology* **58**, 953-972 (2015).
4. Crockford, P. W. et al. Triple oxygen isotope evidence for limited mid-Proterozoic primary productivity. *Nature* **559**, 613-616 (2018).
5. Brocks, J. J. et al. The rise of algae in Cryogenian oceans and the emergence of animals. *Nature* **548**, 578-581 (2017).
6. Wang, X., Dong, L., Ma, H., Lang, X. & Wang, R. Primary productivity recovery and shallow-water oxygenation during the Sturtian deglaciation in South China. *Global Planet. Change* **241**, 104546 (2024).
7. Lenton, T. M., Boyle, R. A., Poulton, S. W., Shields-Zhou, G. A. & Butterfield, N. J. Co-evolution of eukaryotes and ocean oxygenation in the Neoproterozoic era. *Nat. Geosci.* **7**, 257-265 (2014).
8. Tziperman, E., Halevy, I., Johnston, D. T., Knoll, A. H. & Schrag, D. P. Biologically induced initiation of Neoproterozoic snowball-Earth events. *Proc. Natl Acad. Sci.* **108**, 15091-15096 (2011).
9. Rothman, D. H., Hayes, J. M. & Summons, R. E. Dynamics of the Neoproterozoic carbon cycle. *Proc. Natl Acad. Sci.* **100**, 8124-8129 (2003).
10. Feulner, G., Hallmann, C. & Kienert, H. Snowball cooling after algal rise. *Nat. Geosci.* **8**, 659-662 (2015).
11. Kump, L. R. The rise of atmospheric oxygen. *Nature* **451**, 277-278 (2008).
12. Planavsky, N. J. et al. Widespread iron-rich conditions in the mid-Proterozoic ocean. *Nature* **477**, 448-451 (2011).
13. Liu, P. et al. Large influence of dust on the Precambrian climate. *Nat. Commun.* **11**, 4427 (2020).
14. Motomura, K. et al. The nitrate-limited freshwater environment of the late Paleoproterozoic Embury Lake Formation, Flin Flon belt, Canada. *Chem. Geol.* **616**, 121234 (2023).
15. Kang, J., Gill, B., Reid, R., Zhang, F. & Xiao, S. Nitrate limitation in early Neoproterozoic oceans delayed the ecological rise of eukaryotes. *Sci. Adv.* **9**, eade9647 (2023).
16. Laakso, T. A. & Schrag, D. P. A small marine biosphere in the Proterozoic. *Geobiol.* **17**, 161-171 (2019).
17. Guilbaud, R. et al. Phosphorus-limited conditions in the early Neoproterozoic ocean maintained low levels of atmospheric oxygen. *Nat. Geosci.* **13**, 296-301 (2020).
18. Planavsky, N. J. et al. The evolution of the marine phosphate reservoir. *Nature* **467**, 1088-1090 (2010).

19. Cebrian, J., Stutes, A. L. & Corcoran, A. A. Effects of nutrient enrichment and shading on sediment primary production and metabolism in eutrophic estuaries. *Mar. Ecol. Prog. Ser.* **312**, 29-43 (2006).
20. Estes, J. A. et al. Trophic Downgrading of Planet Earth. *Science* **333**, 301-306 (2011).
21. Eckford-Soper, L. K., Andersen, K. H., Hansen, T. F. & Canfield, D. E. A case for an active eukaryotic marine biosphere during the Proterozoic era. *Proc. Natl Acad. Sci.* **119**, e2122042119 (2022).
22. Laakso, T. A. & Schrag, D. A theory of atmospheric oxygen. *Geobiol.* **15**, 366-384 (2017).
23. Claire, M. W., Catling, D. C. & Zahnle, K. J. Biogeochemical modelling of the rise in atmospheric oxygen. *Geobiol.* **4**, 239-269 (2006).
24. Gianchandani, K., Halevy, I., Gildor, H., Ashkenazy, Y. & Tziperman, E. Production of Neoproterozoic banded iron formations in a partially ice-covered ocean. *Nat. Geosci.*, 1-4 (2024).
25. Ramme, L., Ilyina, T. & Marotzke, J. Moderate greenhouse climate and rapid carbonate formation after Marinoan snowball Earth. *Nat. Commun.* **15**, 3571 (2024).
26. Cao, X. et al. Earth's tectonic and plate boundary evolution over 1.8 billion years. *Geosci. Front.* **15**, 101922 (2024).
27. Li, Z.-X. et al. Assembly, configuration, and break-up history of Rodinia: a synthesis. *Precambrian Res.* **160**, 179-210 (2008).
28. Liu, P., Liu, Y., Gu, S., Hoffman, P. & Li, S. A positive cooling feedback for the Neoproterozoic snowball Earth initiation due to weakening of ocean ventilation. *Geophys. Res. Lett.* **50**, e2022GL102020 (2023).
29. Long, M. C. et al. Simulations with the marine biogeochemistry library (MARBL). *J. Adv. Model. Earth Syst.* **13**, e2021MS002647 (2021).
30. Sims, P. A., Mann, D. G. & Medlin, L. K. Evolution of the diatoms: insights from fossil, biological and molecular data. *Phycologia* **45**, 361-402 (2006).
31. Steinberg, D. K. & Landry, M. R. Zooplankton and the ocean carbon cycle. *Annu. Rev. Mar. Science* **9**, 413-444 (2017).
32. Holder, C. & Gnanadesikan, A. How well do Earth System Models capture apparent relationships between phytoplankton biomass and environmental variables? *Global Biogeochem. Cycles* **37**, e2023GB007701 (2023).
33. Marinov, I., Doney, S. & Lima, I. Response of ocean phytoplankton community structure to climate change over the 21st century: partitioning the effects of nutrients, temperature and light. *Biogeosciences* **7**, 3941-3959 (2010).
34. Beckmann, A. & Hense, I. Beneath the surface: Characteristics of oceanic ecosystems under weak mixing conditions – A theoretical investigation. *Prog. Oceanogr.* **75**, 771-796 (2007).
35. Holmer, M. & Bondgaard, E. J. Photosynthetic and growth response of eelgrass to low oxygen and high sulfide concentrations during hypoxic events. *Aquat. Bot.* **70**, 29-38 (2001).
36. Twilley, R. R., Kemp, W. M., Staver, K. W., Stevenson, J. C. & Boynton, W. R. Nutrient enrichment of estuarine submersed vascular plant communities. 1. Algal growth and effects on production of plants and associated communities. *Marine ecology progress series. Oldendorf* **23**, 179-191 (1985).
37. Moore, J. K., Doney, S. C. & Lindsay, K. Upper ocean ecosystem dynamics and iron cycling in a global three-dimensional model. *Global Biogeochem. Cycles* **18** (2004).
38. Moore, C. et al. Processes and patterns of oceanic nutrient limitation. *Nat. Geosci.* **6**, 701-710 (2013).
39. McGlathery, K. J. Macroalgal blooms contribute to the decline of seagrass in nutrient-enriched coastal waters. *J. Phycol.* **37** (2001).
40. Huntington, B. E. & Boyer, K. E. Effects of red macroalgal (Gracilariopsis sp.) abundance on eelgrass Zostera marina in Tomales Bay, California, USA. *Mar. Ecol. Prog. Ser.* **367**, 133-142 (2008).
41. Churilova, T. Y., Suslin, V., Moiseeva, N. & Efimova, T. Phytoplankton bloom and photosynthetically active radiation in coastal waters. *J. Appl. Spectrosc.* **86**, 1084-1091 (2020).

42. Sarangi, R., Chauhan, P. & Nayak, S. Phytoplankton bloom monitoring in the offshore water of Northern Arabian Sea using IRS-P4 OCM Satellite data. (2001).
43. Raghavan, B. et al. in *Remote Sensing of the Marine Environment.* 236-242 (SPIE).
44. Heck Jr., K. L., Pennock, J. R., Valentine, J. F., Coen, L. D. & Sklenar, S. A. Effects of nutrient enrichment and small predator density on seagrass ecosystems: An experimental assessment. *Limnol. Oceanogr.* **45**, 1041-1057 (2000).
45. Shiomoto, A., Tadokoro, K., Nagasawa, K. & Ishida, Y. Trophic relations in the subarctic North Pacific ecosystem: possible feeding effect from pink salmon. *Mar. Ecol. Prog. Ser.* **150**, 75-85 (1997).
46. Odate, T. Plankton abundance and size structure in the northern North Pacific Ocean in early summer. *Fish. Oceanogr.* **3**, 267-278 (1994).
47. Carpenter, S. R. et al. Trophic cascades, nutrients, and lake productivity: whole-lake experiments. *Ecol. Monogr.* **71**, 163-186 (2001).
48. Okey, T. A. et al. Simulating community effects of sea floor shading by plankton blooms over the West Florida Shelf. *Ecol. Model.* **172**, 339-359 (2004).
49. Meyercordt, J. & Meyer-Reil, L.-A. Primary production of benthic microalgae in two shallow coastal lagoons of different trophic status in the southern Baltic Sea. *Mar. Ecol. Prog. Ser.* **178**, 179-191 (1999).
50. Morel, A. & Bricaud, A. Theoretical results concerning light absorption in a discrete medium, and application to specific absorption of phytoplankton. *Deep Sea Research Part A. Oceanographic Research Papers* **28**, 1375-1393 (1981).
51. Deng, L. et al. Estimation of vertical size-fractionated phytoplankton primary production in the northern South China Sea. *Ecol. Indic.* **135**, 108546 (2022).
52. Sciascia, R., De Monte, S. & Provenzale, A. Physics of sinking and selection of plankton cell size. *Phys. Lett. A* **377**, 467-472 (2013).
53. Mills, D. B., Vuillemin, A., Muschler, K., Coskun, Ö. K. & Orsi, W. D. The Rise of Algae promoted eukaryote predation in the Neoproterozoic benthos. *Sci. Adv.* **11**, eadt2147 (2025).
54. Lewis, M. R., Carr, M.-E., Feldman, G. C., Esaias, W. & McClain, C. Influence of penetrating solar radiation on the heat budget of the equatorial Pacific Ocean. *Nature* **347**, 543-545 (1990).
55. Krüger, O. & Graßl, H. Southern Ocean phytoplankton increases cloud albedo and reduces precipitation. *Geophys. Res. Lett.* **38** (2011).
56. Wang, S., Maltrud, M. E., Burrows, S. M., Elliott, S. M. & Cameron-Smith, P. Impacts of Shifts in Phytoplankton Community on Clouds and Climate via the Sulfur Cycle. *Global Biogeochem. Cycles* **32**, 1005-1026 (2018).
57. Mitchell, R. N. & Kirscher, U. Mid-Proterozoic day length stalled by tidal resonance. *Nat. Geosci.* **16**, 567-569 (2023).
58. Zhou, M. et al. Earth-Moon dynamics from cyclostratigraphy reveals possible ocean tide resonance in the Mesoproterozoic era. *Sci. Adv.* **10**, eadn7674 (2024).
59. Laakso, T. A. & Schrag, D. P. Regulation of atmospheric oxygen during the Proterozoic. *Earth Planet. Sci. Lett.* **388**, 81-91 (2014).
60. Rickaby, R. E. M. & Eason Hubbard, M. R. Upper ocean oxygenation, evolution of RuBisCO and the Phanerozoic succession of phytoplankton. *Free Radic. Biol. Med.* **140**, 295-304 (2019).
61. Yee, D. P. et al. The V-type ATPase enhances photosynthesis in marine phytoplankton and further links phagocytosis to symbiogenesis. *Curr. Biol.* **33**, 2541-2547.e2545 (2023).
62. Armstrong, R. A., Lee, C., Hedges, J. I., Honjo, S. & Wakeham, S. G. A new, mechanistic model for organic carbon fluxes in the ocean based on the quantitative association of POC with ballast minerals. *Deep Sea Res. Part II* **49**, 219-236 (2002).
63. Letscher, R. T., Moore, J. K., Teng, Y.-C. & Primeau, F. Variable C: N: P stoichiometry of dissolved organic matter cycling in the Community Earth System Model. *Biogeosciences* **12**, 209-221 (2015).
64. Li, X. et al. A high-resolution climate simulation dataset for the past 540 million years. *Sci. Data* **9**, 1-10 (2022).

65. Liu, Y. et al. Spatial continuous modeling of early Cenozoic carbon cycle and climate. *Natl. Sci. Rev.* **11**, nwae061 (2024).
66. Hurrell, J. W. et al. The community earth system model: a framework for collaborative research. *Bull. Am. Meteorol. Soc.* **94**, 1339-1360 (2013).
67. Smith, R. et al. The parallel ocean program (POP) reference manual: ocean component of the community climate system model (CCSM) and community earth system model (CESM). *Rep. LAUR-01853* **141**, 1-140 (2010).
68. Smith, R. D. & McWilliams, J. C. Anisotropic horizontal viscosity for ocean models. *Ocean Modell.* **5**, 129-156 (2003).
69. Gent, P. R. & Mcwilliams, J. C. Isopycnal Mixing in Ocean Circulation Models. *J. Phys. Oceanogr.* **20**, 150-155 (1990).
70. Liu, Y., Peltier, W., Yang, J. & Vettoretti, G. The initiation of Neoproterozoic "snowball" climates in CCSM3: the influence of paleocontinental configuration. *Clim. Past* **9**, 2555-2577 (2013).
71. Large, W. G., McWilliams, J. C. & Doney, S. C. Oceanic vertical mixing: A review and a model with a nonlocal boundary layer parameterization. *Rev. Geophys.* **32**, 363-403 (1994).
72. Baatsen, M. et al. The middle to late Eocene greenhouse climate modelled using the CESM 1.0. 5. *Clim. Past* **16**, 2573-2597 (2020).
73. Moore, J. K., Doney, S. C., Kleypas, J. A., Glover, D. M. & Fung, I. Y. An intermediate complexity marine ecosystem model for the global domain. *Deep Sea Res. Part II* **49**, 403-462 (2002).
74. Séférian, R. et al. Tracking improvement in simulated marine biogeochemistry between CMIP5 and CMIP6. *Curr. Clim. Change Rep.* **6**, 95-119 (2020).
75. Molina, E., Martínez, M., Sánchez, S., García, F. & Contreras, A. Growth and biochemical composition with emphasis on the fatty acids of Tetraselmis sp. *Appl. Microbiol. Biotechnol.* **36**, 21-25 (1991).
76. Anderson, L. A. On the hydrogen and oxygen content of marine phytoplankton. *Deep Sea Res. Part I* **42**, 1675-1680 (1995).
77. Sharoni, S. & Halevy, I. Geologic controls on phytoplankton elemental composition. *Proc. Natl Acad. Sci.* **119**, e2113263118 (2022).
78. Penn, J. L., Deutsch, C., Payne, J. L. & Sperling, E. A. Temperature-dependent hypoxia explains biogeography and severity of end-Permian marine mass extinction. *Science* **362**, eaat1327 (2018).
79. Bohlen, L., Dale, A. W. & Wallmann, K. Simple transfer functions for calculating benthic fixed nitrogen losses and C:N:P regeneration ratios in global biogeochemical models. *Global Biogeochem. Cycles* **26** (2012).
80. Soetaert, K., Herman, P. M. & Middelburg, J. J. A model of early diagenetic processes from the shelf to abyssal depths. *Geochim. Cosmochim. Acta* **60**, 1019-1040 (1996).
81. Dunne, J. P., Sarmiento, J. L. & Gnanadesikan, A. A synthesis of global particle export from the surface ocean and cycling through the ocean interior and on the seafloor. *Global Biogeochem. Cycles* **21** (2007).
82. Moore, J. K., Lindsay, K., Doney, S. C., Long, M. C. & Misumi, K. Marine Ecosystem Dynamics and Biogeochemical Cycling in the Community Earth System Model [CESM1(BGC)]: Comparison of the 1990s with the 2090s under the RCP4.5 and RCP8.5 Scenarios. *J. Clim.* **26**, 9291-9312 (2013).
83. Doney, S. C. et al. Mechanisms governing interannual variability in upper-ocean inorganic carbon system and air–sea CO2 fluxes: Physical climate and atmospheric dust. *Deep Sea Res. Part II* **56**, 640-655 (2009).
84. Long, M. C., Lindsay, K., Peacock, S., Moore, J. K. & Doney, S. C. Twentieth-century oceanic carbon uptake and storage in CESM1 (BGC). *J. Clim.* **26**, 6775-6800 (2013).
85. Park, Y. et al. Emergence of the Southeast Asian islands as a driver for Neogene cooling. *Proc. Natl Acad. Sci.* **117**, 25319-25326 (2020).

86. Zuo, H. et al. A revised model of global silicate weathering considering the influence of vegetation cover on erosion rate. *Geosci. Model Dev.* **17**, 3949-3974 (2024).
87. Gabet, E. J. & Mudd, S. M. A theoretical model coupling chemical weathering rates with denudation rates. *Geology* **37**, 151-154 (2009).
88. Tang, M., Chu, X., Hao, J. & Shen, B. Orogenic quiescence in Earth's middle age. *Science* **371**, 728-731 (2021).
89. Morris, J. L. et al. The timescale of early land plant evolution. *Proc. Natl Acad. Sci.* **115**, E2274-E2283 (2018).
90. Gough, D. Solar interior structure and luminosity variations. *Sol. Phys.* **74**, 21-34 (1981).
91. Liu, Y., Liu, P., Li, D., Peng, Y. & Hu, Y. Influence of dust on the initiation of Neoproterozoic snowball Earth events. *J. Clim.* **34**, 6673-6689 (2021).
92. Jickells, T. et al. Global iron connections between desert dust, ocean biogeochemistry, and climate. *Science* **308**, 67-71 (2005).
93. Solmon, F., Chuang, P., Meskhidze, N. & Chen, Y. Acidic processing of mineral dust iron by anthropogenic compounds over the north Pacific Ocean. *J. Geophys. Res.: Atmos.* **114** (2009).
94. Hand, J. et al. Estimates of atmospheric-processed soluble iron from observations and a global mineral aerosol model: Biogeochemical implications. *J. Geophys. Res.: Atmos.* **109** (2004).
95. Kasting, J. & Walker, J. C. Limits on oxygen concentration in the prebiological atmosphere and the rate of abiotic fixation of nitrogen. *J. Geophys. Res.: Oceans* **86**, 1147-1158 (1981).
96. Kasting, J. F. Stability of ammonia in the primitive terrestrial atmosphere. *J. Geophys. Res.: Oceans* **87**, 3091-3098 (1982).
97. Liu, P. et al. Triple oxygen isotope constraints on atmospheric O_2 and biological productivity during the mid-Proterozoic. *Proc. Natl Acad. Sci.* **118**, e2105074118 (2021).
98. Mather, T. et al. Nitric acid from volcanoes. *Earth Planet. Sci. Lett.* **218**, 17-30 (2004).
99. Johnson, B. & Goldblatt, C. The nitrogen budget of Earth. *Earth Sci. Rev.* **148**, 150-173 (2015).
100. Hartmann, J., Dürr, H. H., Moosdorf, N., Meybeck, M. & Kempe, S. The geochemical composition of the terrestrial surface (without soils) and comparison with the upper continental crust. *Int. J. Earth Sci.* **101**, 365-376 (2012).
101. Watanabe, Y., Tajika, E. & Ozaki, K. Evolution of iron and oxygen biogeochemical cycles during the Precambrian. *Geobiol.* **21**, 689-707 (2023).
102. Hartmann, J., Moosdorf, N., Lauerwald, R., Hinderer, M. & West, A. J. Global chemical weathering and associated P-release—The role of lithology, temperature and soil properties. *Chem. Geol.* **363**, 145-163 (2014).
103. Lucas, D. et al. Failure analysis of parameter-induced simulation crashes in climate models. *Geosci. Model Dev.* **6**, 1157-1171 (2013).

Acknowledgments

Y.L. is supported by the National Natural Science Foundation of China under grant 42225606. P.L is supported by the National Natural Science Foundation of China under grant 42475052, the National Key Research and Development Program of China under grant 2024YFF0808000, Fundamental Research Funds for the Central Universities under grant 202541010, and Young Talent of Lifting Engineering for Science and Technology in Shandong, China under grant SDAST2024QTA022. S.L. is supported by the National Natural Science Foundation of China under grant 42121005. The simulations were performed on the High-performance Computing Platform of Peking University and Marine Big Data Center of Institute for Advanced Ocean Study of Ocean University of China. We thank for the technical support of the National Large Scientific and Technological Infrastructure "Earth System Numerical Simulation Facility" (https://cstr.cn/31134.02.EL).

Author Contributions

Y.L. proposed the project. P.L. and Y.L. performed modeling analyses. P.L. and Y.L. wrote the manuscript. L.D., J.Z., S.L., and Y.C. contributed to the discussion and manuscript revision.

Competing Interests

Authors declare that they have no competing interests.

Figures Legends

Fig. 1. Simulated chlorophyll and plankton carbon in preindustrial (PI) and Proterozoic conditions. (A-C) Annual mean chlorophyll distributions averaged within the upper 150 m and (D-F) zonal mean plankton carbon amount within the upper ocean in the preindustrial condition (top), warm (pCO_2=2240 ppmv, middle), and cold (pCO_2=280 ppmv, bottom) scenarios in the Proterozoic. The grey contour lines in A-C and light green bars at the top of D-F indicate the edges and areas of sea ice with the gridbox fraction of 15%, respectively.

Fig. 2. Simulated net primary productivity and light availability in preindustrial (PI) and Proterozoic conditions. (A-C) Annual mean net primary productivity averaged within the upper 150 m, (D-F) zonal mean net primary productivity within the upper ocean, and (G-I) light availability within the upper ocean in the preindustrial condition (top), warm (pCO_2=2240 ppmv, middle), and cold (pCO_2=280 ppmv, bottom) scenarios in the Proterozoic. The green contour lines in A-C and light green bars at the top of D-I indicate the edges and areas of sea ice with the gridbox fraction of 15%, respectively.

Fig. 3. Simulated sunlight and limiting factors for marine productivity in preindustrial (PI) and Proterozoic conditions. (A-C) Annual mean photosynthesis-available radiation in the 10-20 m (second) ocean layer and (D-F) spatial distribution of the factor that most limits annual growth averaged within the upper 150 m for the small phytoplankton in the preindustrial condition (top), warm (pCO_2=2240 ppmv, middle), and cold (pCO_2=280 ppmv, bottom) scenarios in the Proterozoic. The green contour lines in each panel indicate the edges of sea ice with the gridbox fraction of 15%.

Fig. 4. Schematic diagrams showing the simulated greener but less productive Proterozoic ocean compared to preindustrial (PI). (A) and (B) represent the simulation results in tropical regions for PI and warm Proterozoic (pCO_2=2240 ppmv), respectively. The contours on the horizontal plane in both panels show the chlorophyll levels (unit: mg/m^3) in the surface ocean. The contours on the left and right sides show the vertical distribution of the meridionally averaged radiation (unit: W/m^2) and zonally averaged net primary productivity (NPP) (unit: 10^{-7} mmol/m^3/s), respectively. The atmospheric oxygen level (pO_2) in the Proterozoic simulation (B) is 1% of the present level. Two panels share the same color bar as shown in the figure.

Editorial Summary:
Here, the authors leverage the Earth system model CESM1.2.2 to simulate Proterozoic marine biogeochemical cycles. Their simulations suggest that dense phytoplankton at the surface would have created a greener ocean which may have prevented sunlight from reaching subsurface levels and contributed to reduced ocean productivity.

Peer Review Information: *Nature Communications* thanks the anonymous, reviewer(s) for their contribution to the peer review of this work. A peer review file is available."

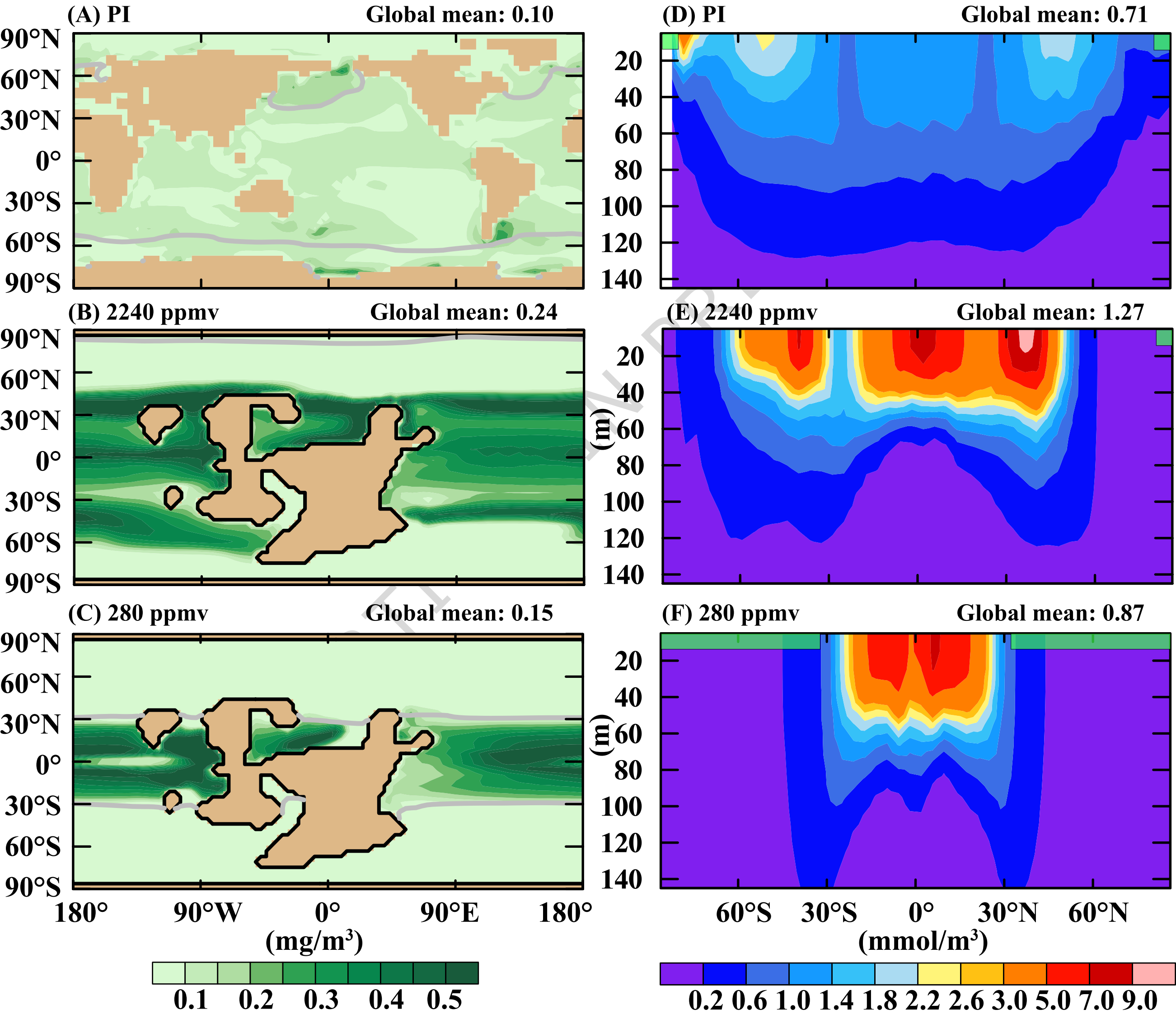

(A) PI
Global mean: 0.10
(B) 2240 ppmv
Global mean: 0.24
(C) 280 ppmv
Global mean: 0.15
90°N
60°N
30°N
0°
30°S
60°S
90°S
180°
90°W
0°
90°E
180°
(mg/m³)
0.1
0.2
0.3
0.4
0.5
(D) PI
Global mean: 0.71
(E) 2240 ppmv
Global mean: 1.27
(F) 280 ppmv
Global mean: 0.87
(m)
20
40
60
80
100
120
140
60°S
30°S
0°
30°N
60°N
(mmol/m³)
0.2
0.6
1.0
1.4
1.8
2.2
2.6
3.0
5.0
7.0
9.0

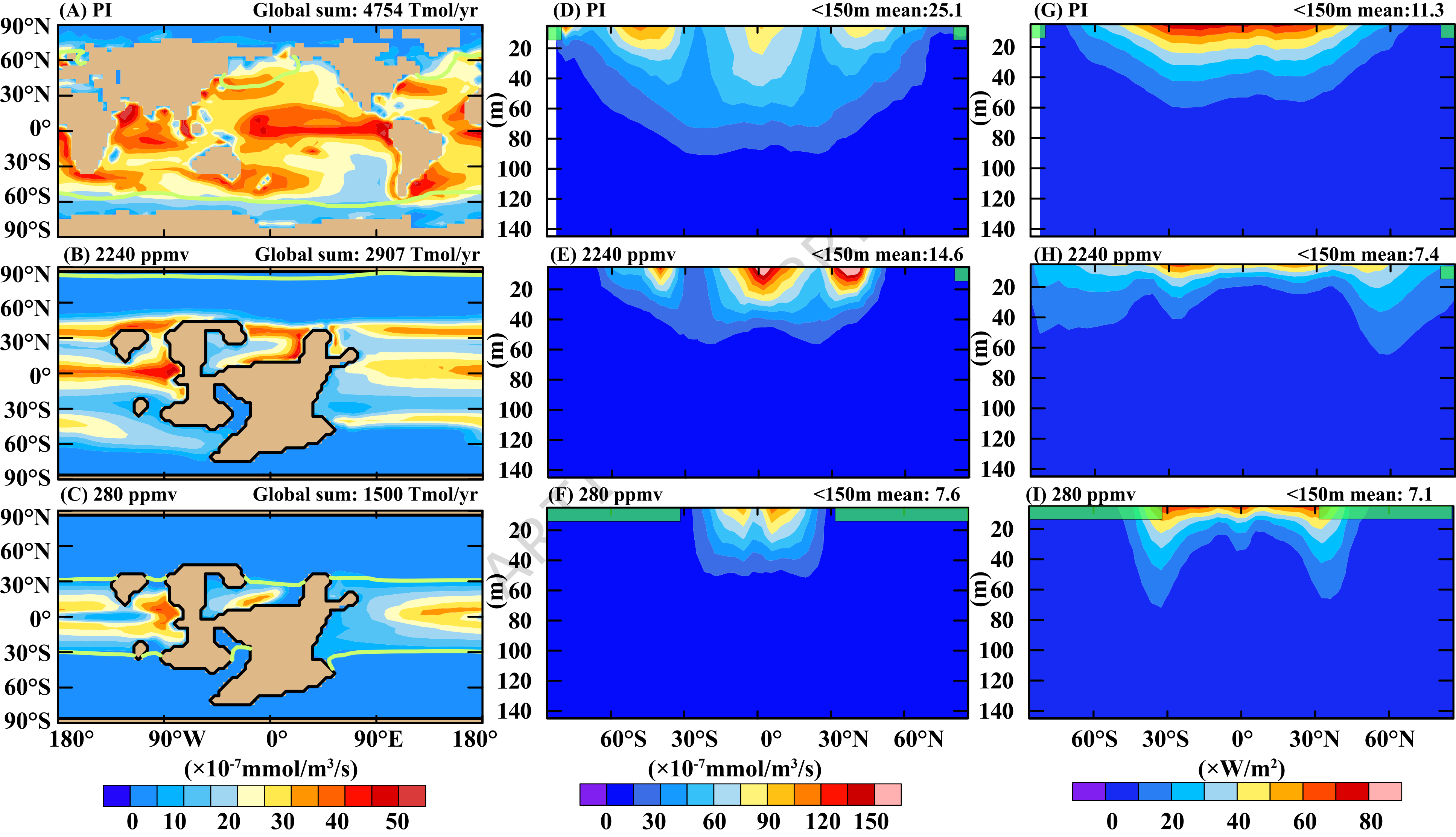
(A) PI
Global sum: 4754 Tmol/yr
(B) 2240 ppmv
Global sum: 2907 Tmol/yr
(C) 280 ppmv
Global sum: 1500 Tmol/yr
90°N 60°N 30°N 0° 30°S 60°S 90°S
180° 90°W 0° 90°E 180°
(×10⁻⁷mmol/m³/s)
0 10 20 30 40 50
(D) PI
<150m mean:25.1
(E) 2240 ppmv
<150m mean:14.6
(F) 280 ppmv
<150m mean: 7.6
(m)
20 40 60 80 100 120 140
60°S 30°S 0° 30°N 60°N
(×10⁻⁷mmol/m³/s)
0 30 60 90 120 150
(G) PI
<150m mean:11.3
(H) 2240 ppmv
<150m mean:7.4
(I) 280 ppmv
<150m mean: 7.1
(×W/m²)
0 20 40 60 80

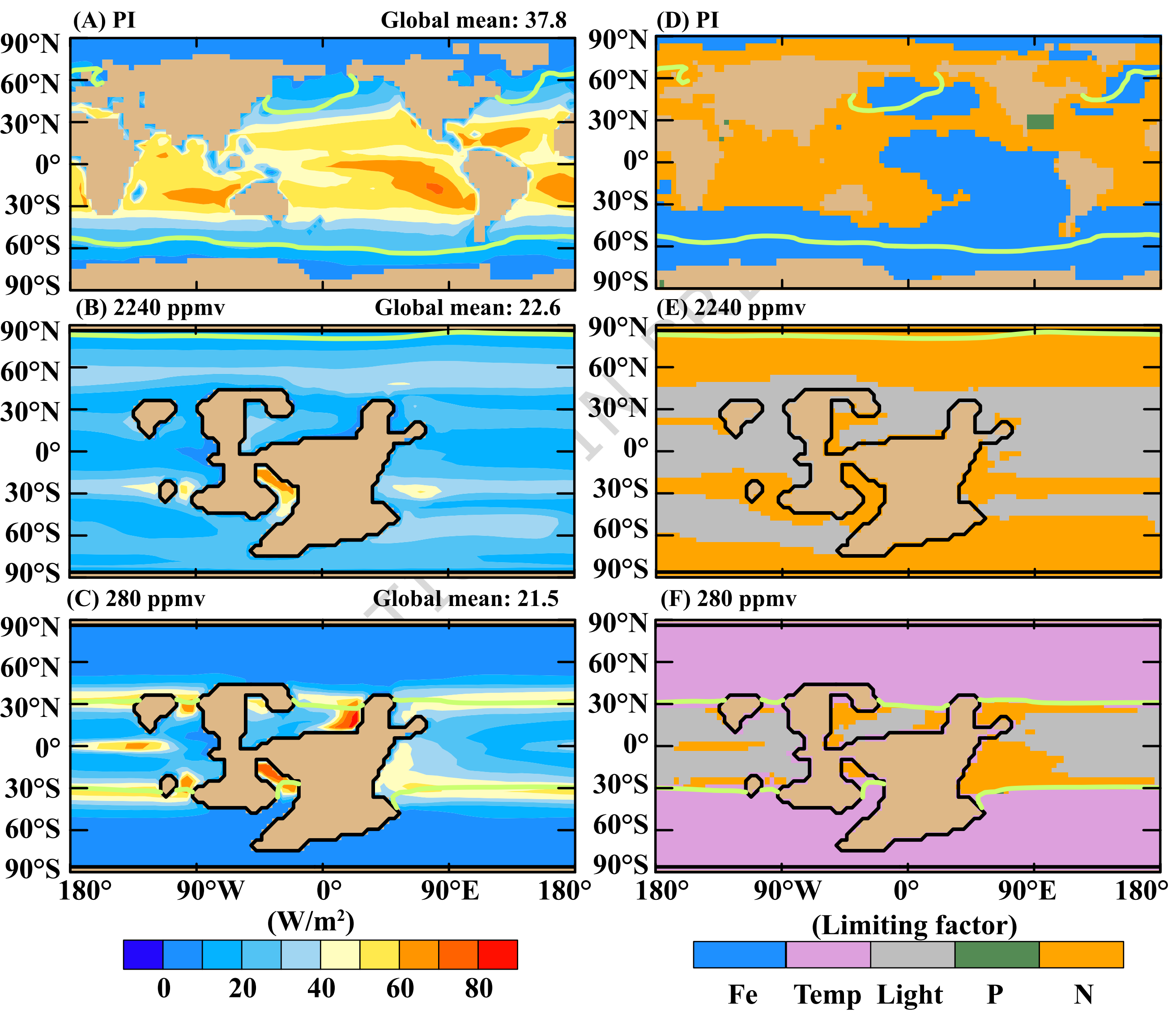
(A) PI
Global mean: 37.8
(B) 2240 ppmv
Global mean: 22.6
(C) 280 ppmv
Global mean: 21.5
(D) PI
(E) 2240 ppmv
(F) 280 ppmv
90°N
60°N
30°N
0°
30°S
60°S
90°S
180°
90°W
0°
90°E
180°
(W/m²)
0
20
40
60
80
(Limiting factor)
Fe
Temp
Light
P
N

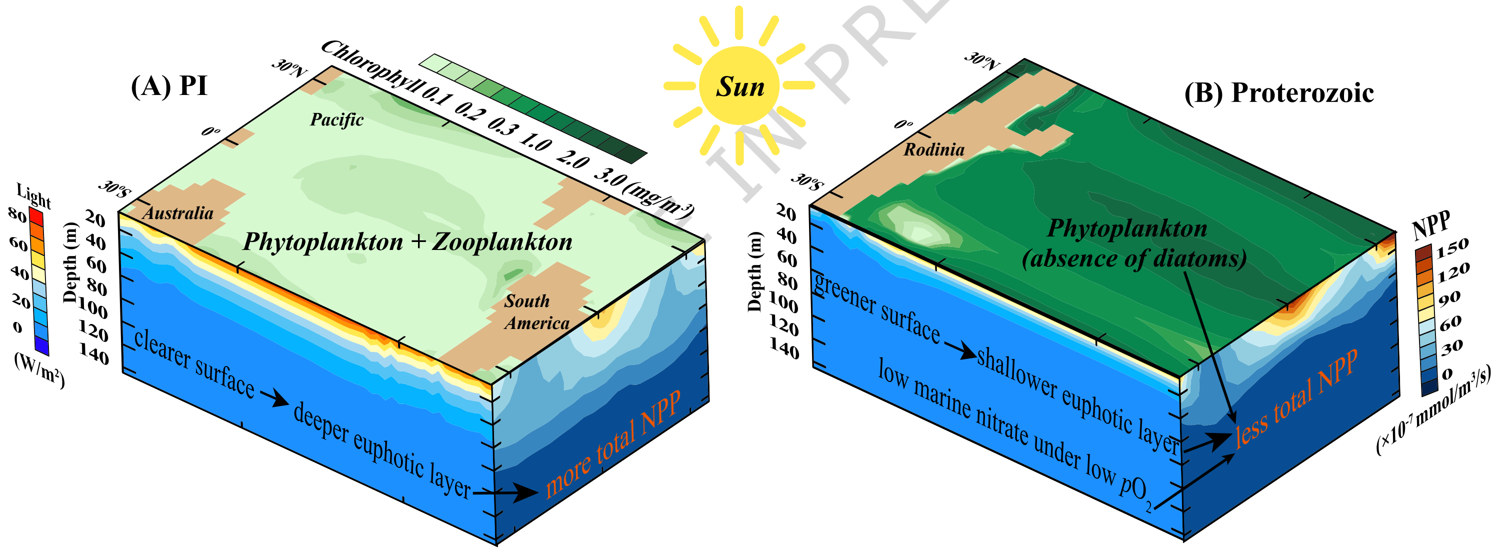
(A) PI
Chlorophyll 0.1 0.2 0.3 1.0 2.0 3.0 (mg/m³)
Sun
(B) Proterozoic
30°N
0°
30°S
Pacific
Australia
Phytoplankton + Zooplankton
South America
Light
80
60
40
20
0
(W/m²)
Depth (m)
20
40
60
80
100
120
140
clearer surface
deeper euphotic layer
more total NPP
Rodinia
Phytoplankton
(absence of diatoms)
greener surface
shallower euphotic layer
low marine nitrate under low pO2
less total NPP
NPP
150
120
90
60
30
0
(×10⁻⁷ mmol/m³/s)